THE EFFECT OF ARTIFICIAL AMALGAMATES ON IDENTIFYING PATHOGENESIS

Philip Naveen

August 28, 2021

ABSTRACT

The purpose of this research was to define acceleration in diagnostic procedures for airborne diseases. Airborne pathogenicity can be troublesome to diagnose due to intrinsic variation and overlapping symptoms. Coronavirus testing was an instance of a flawed diagnostic biomarker. The levels of independent variables (IV) were vanilla, sparse, and dense amalgamates formed from multilayer perceptrons and image processing algorithms. The dependent variable (DV) was the classification accuracy. It was hypothesized that if a dense amalgamate is trained to identify Coronavirus, the accuracy would be the highest. The amalgamates were trained to analyze the morphological patches within radiologist-verified medical imaging retrieved from online databanks. Using cross-validation simulations augmented with machine-learning, the DV was consulted for each amalgamate. Self-calculated t-tests supported the research hypothesis, with the dense amalgamate achieving 85.37% correct classification rate. The null hypothesis was rejected. Flaws within the databanks were possible sources of error. A new multivariate algorithm invented here performed better than the IV. It identified Coronavirus and other airborne diseases from 96-99% accuracy. The model was also adept in identifying heterogeneity and malignancy of lung cancer as well as differentiating viral and bacterial pathogenicity of infections. Future modifications would involve extending the algorithm to diseases in other anatomical structures such as osteopenia/osteoporosis in the vertebral column.

1 Introduction

Significant medical advances in the past century have led to improvements to diagnostic procedures and technology. One example is the development of biomarkers, which are biological altercations within organisms indicative of pathogenicity. These are often grouped into panels for disease diagnosis. Biomarkers vary in cost and implementation. The most successful biomarkers are used in the medical field to test for disease via measuring unique pathogenic effects. While biomarkers are dependable, they are costly to develop, and require extended testing. The low success rate of manufacturing successful biomarkers accompanied by the long timeframe of development leads to the spread of pandemics (He et al, 2020).

One example of this occurring was COVID-19, which is known by most as the Coronavirus. Coronavirus has three spike protein variants: SARS-CoV, SARS-CoV-2, and MERS-CoV (He et al, 2020). Across the three variants, the main side effects are very similar to Influenza, Tuberculosis, and Pneumonia on the surface (Liu et al, 2020). Throughout 2020 and early 2021, the United States had incredible difficulty differentiating infected and healthy individuals. Hospitals were overloaded beyond their carrying capacities. Coronavirus testing was unreliable and rushed. Many people waited weeks for their results due to the extensive analysis of the samples required for proper diagnosis (Simoneaux and Shafer, 2020). Luckily, the vaccinations are currently fixing the issue. The effects are still prominent in very populated areas such as India because the lack of fast diagnosis leads to extended lockdowns. Post-Coronavirus, other pandemics could yield similar effects due to the slowness of testing. The Delta and Lambda variants are examples of how intrinsic mutation can be troublesome for developing biomarkers (He et al, 2020; Liu et al, 2020). If better diagnostic procedures could be implemented, the curve-flattening process would be much easier.

Computed tomography (CT) and x-ray scans are used by radiologists to image anatomical structures within humans non-invasively (Sapthagirivasan and Anburajan, 2013). Generally, airborne diseases have prominent pathogenic effects

in the lungs (Liu et al, 2020). CT scans and x-rays can show inflammatory patches in those regions (Wang et al, 2020). Unfortunately, there are only an estimated 34,000 radiologists in the USA, meaning that using the aforementioned diagnostic procedures may be difficult depending on the area. This research attempts to develop a method for diagnosing Coronavirus without radiologists. Theoretically, if a computational application can identify COVID-19 using medical imaging, then testing for diseases will become more widespread and efficient (Rahimzadeh and Attar, 2020). An artificial intelligence and computational biology approach may be successful.

The independent variable (IV) in this experiment is the type of computational amalgamate used. The computational amalgamates referenced in this research are different permutations of multilayer perceptrons concatenated with image processing via graph theory and computer code. The amalgamates here will be based on machine-learning with optimized feature extraction and classification. Multilayer perceptrons, often referred to as neural-networks, are a framework of nodes connected with synaptic weights being finetuned using backpropagation, which is a process in which every synaptic weight throughout the network is adjusted across many iterations (Baker et al, 2017). Vanilla multilayer perceptrons are the regular formation of backpropagation, which involves the calculation of gradient and loss to optimize the arrangement to solve problems such as regression and classification. Sparse variants have certain nodes with their synapses severed, and dense variants have additional layers with more synaptic weights (Baker et al, 2017). The processing algorithms here cropped the image and lessened the pixel density, since those operations are conventionally used when classifying images (Albawi and Mohammed, 2017).

In this experiment, the dependent variable (DV) is the correct classification rate of COVID-19 returned when classifying Coronavirus-infected lungs. The correct classification rate will be represented as the accuracy. The DV will be measured via a specialized simulation that will operate based on the training data points generated via an autoencoder, which is an instance of unsupervised learning that augments images based on old data (Xu et al, 2019). A confusion matrix will be used to assess the model (Xu, 2019). For multi-class identification, confusion matrices can be fairly complex, so a one-vs-everything approach was taken here to simplify the statistics (Liu et al, 2017). The four cases will be true positives, true negatives, false positives, and false negatives. The calculation of accuracy is the true positives and true negatives compared against all the predictions (Simoneaux and Shafer, 2020; Xu et al, 2019).

The purpose of this experiment is to determine the effect of different computational amalgamates on the diagnosis of Coronavirus by analyzing CT scans and x-rays of the lung. The levels of IV are vanilla, sparse, and dense amalgamates. The control variable is the vanilla amalgamate. The DV is the accuracy calculated by the confusion matrix. The research hypothesis in this experiment is that if the dense amalgamate is trained on CT scans and x-rays of Coronavirus in the lungs, then it will score higher accuracy than the vanilla and sparse amalgamates. This is based on the fact that the dense multilayer perceptrons have shown to be successful in image classification in the past. If the identification of COVID-19 is successful as was in other studies, then computer-based diagnosis may be promising in differentiating other airborne diseases (Rahimzadeh and Attar, 2020; Wang et al, 2020). The knowledge gained from this experiment can be applied in the creation of a new hybrid multivariate model to accelerate diagnostic procedures for various diseases.

2 Procedure

One Acer laptop with an i7 processor running the 64-bit edition of Windows was obtained. Using Oracle's Virtual Machine (VM) software, a Ubuntu distribution of Linux was forged with Windows being the host. On the VM, Python3 was installed along with JupyterLab. Using Git-Bash and terminal commands, a series of Pip installations were performed to acquire linear algebra and machine-learning dependencies. Through various databanks of COVID-19 images publicly available on Kaggle, medical CT scans and x-rays were downloaded to the VM. Using Python3, image processing algorithms were implemented. The images were cropped to the same size, had their visual acuity reduced to 100x100 pixels per image, and had their third dimension transferred from RGB to GreyScale in the tensor. The refined images were subsequently compared for mean squared error across the classes. Vanilla, sparse, and dense multilayer perceptron models were concatenated to the processing algorithms to form the three amalgamates.

Flowchart 1: Workflow of Simulation System

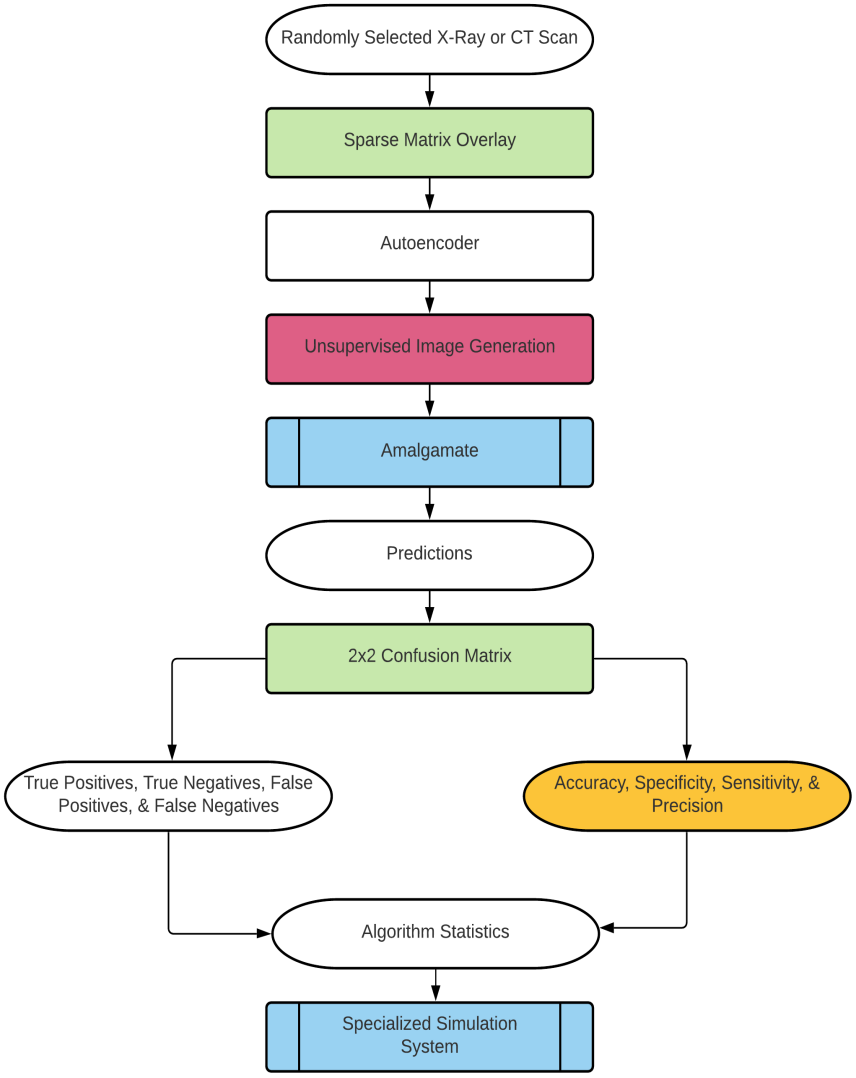

Using the images, the amalgamates were trained for ten epochs and had the cross validation accuracies ignored. A specialized simulation was configured to test the amalgamate performance; the complete workflow of the software simulation can be seen in flowchart 2. Using an autoencoding algorithm trained to generate images, a new batch set of testing images was generated. A one-vs-everything adaptation of a confusion matrix in a 2x2 format was programmed to determine the true positive, true negative, false positive, and false negative prediction values. Each amalgamate had it's performance tested via the simulation system. The data was recorded in the lab notebook. The most accurate of them was determined using a t-test.

Flowchart 2: Workflow of Multivariate Model

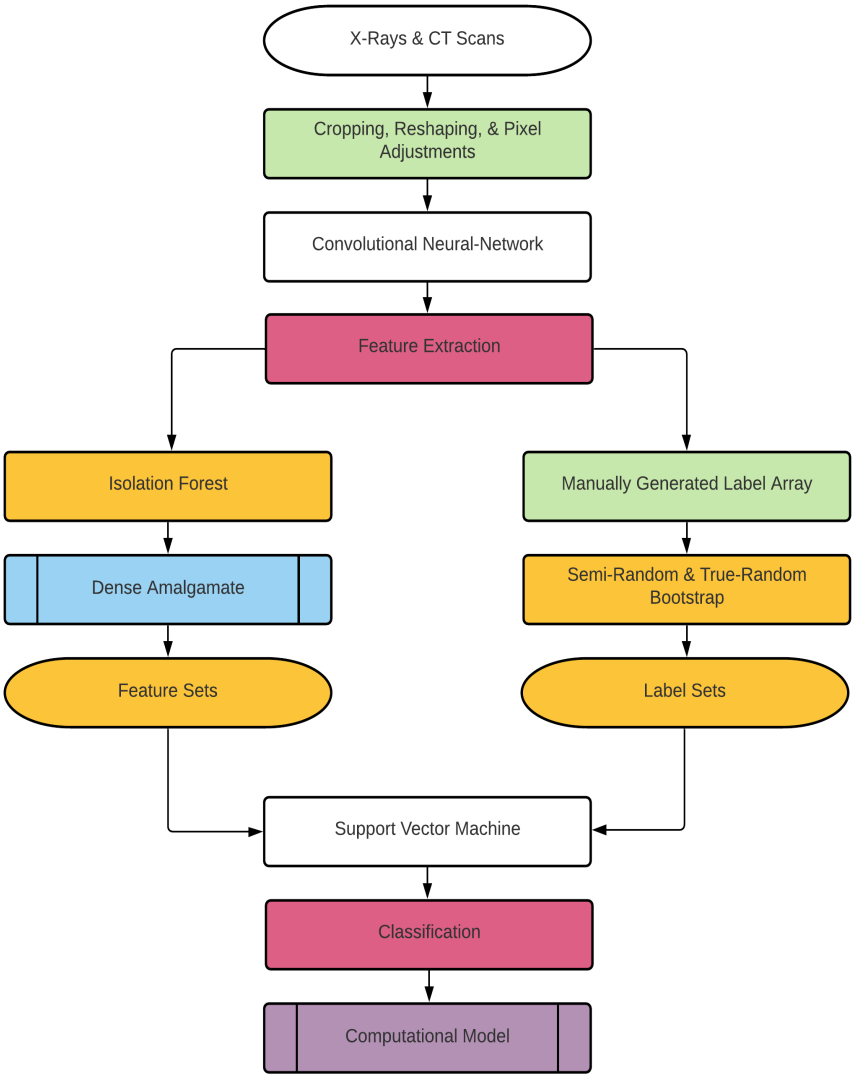

A new hybrid multivariate model was developed here. The morphological patch representations of medical images were analyzed by augmenting the basic dense amalgamate with machine-learning algorithms. A feature extractor was fabricated using a convolutional neural-network. The extractor was developed iteratively based on lightweight pretrained networks such as AlexNet, SqueezeNet, and DenseNet. An isolation forest was configured to eliminate anomaly feature sets extracted from images through unsupervised dimensionality reduction. Through testing many different classification algorithms (e.g. k-means-clustering, k-nearest-neighbors, naive bayes, logistic regressions, support vector machines), an ideal design was determined.

Figure 2: Traditional Classification and One-vs-Everything Classification Patterns

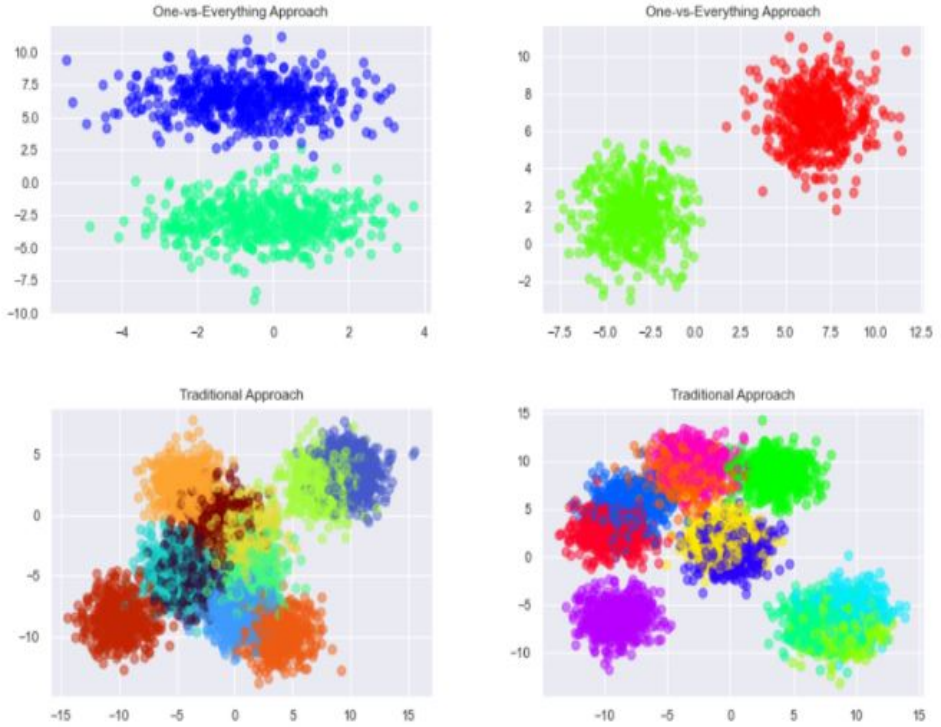

It was found that through splitting a multivariable problem into many binary ones, the computational cost could be lowered and the accuracy could be increased significantly. Through observing a medical professional through shadowing and researching the healthcare system, it was found that developing this algorithm in accordance with electronic health records (EHRs), which are software used by physicians to document information digitally. The model's speed was tested on laptops running i3 (2 cores) and i7 (4+ cores) processors without external graphics processing to replicate the range of computational power the average physician is working with. Through weeks of testing and training the framework, the algorithm was developed to be as integrative as possible.

Figure 1: Five-Stage Variant of the Software Development Life Cycle

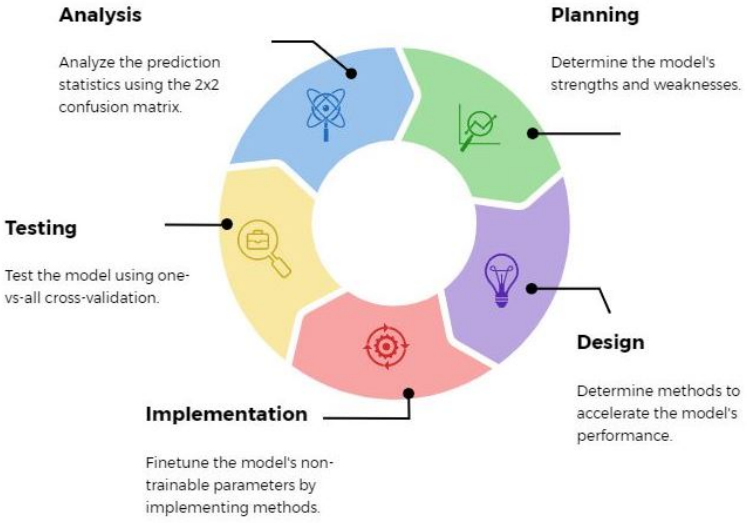

It was programmed using a simplified variant of the software development lifecycle (figure 1), which is a principle of software engineering used by major corporations and government agencies worldwide. A five-stage variation was

implemented here to ensure streamline development. The final architecture of the engineered model can be seen in flowchart one.

Using the same simulation process for measuring COVID-19 diagnosis, this new hybrid model was tested. The model was also expanded to other diseases. It was trained and tested against Tuberculosis, Carcinoma, and Pneumonia images from Kaggle with the aforementioned simulation. It was further tested when differentiating subtypes and malignancy of Carcinomas and identifying the pathogenicity sources of Pneumonia. These results were also recorded in the lab notebook. Post experimentation, the amalgamates, simulation, and hybrid model were bidirectionally saved as PB and H5 files while the VM was disconnected from the host. The files were uploaded onto GitHub for future modification and cross-platform testing.

3 Results

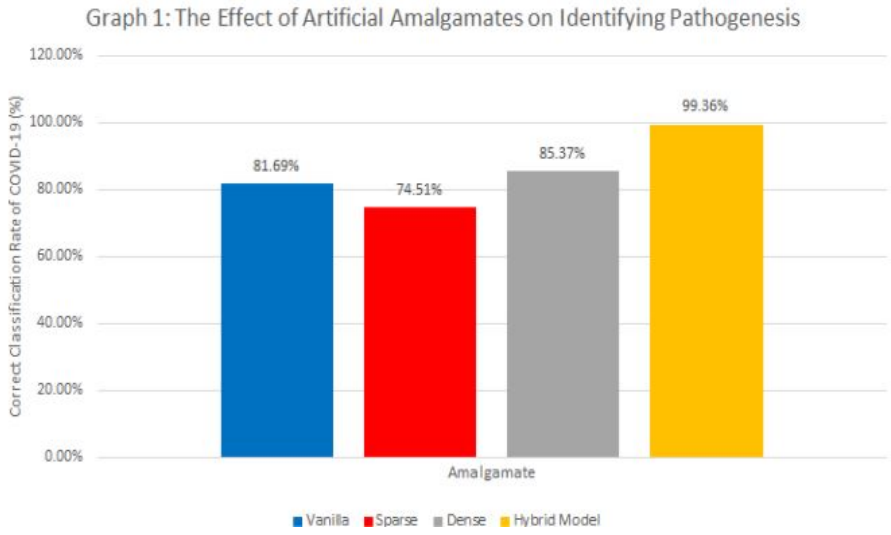

In this research, the effect of computational amalgamates on disease diagnosis was studied and the results of the procedure can be seen in table 1 and graph 1. It was hypothesized the dense amalgamate would yield the highest accuracy when identifying COVID-19. The mean was calculated for each level of independent variables. The mean comparisons of the vanilla (81.69% accuracy), sparse (74.51% accuracy), and dense (85.37% accuracy) amalgamates implied that the dense amalgamate had the highest accuracy, while the sparse one had the lowest. The comparisons supported the research hypothesis. The variances and standard deviation for each level of independent variables were calculated. All six values were very low, which implies the data is precise. There were some outliers when the 1SD, 2SD, and 3SD ranges were consulted. However, those were only considered outliers due to standard deviations being so low.

Table 1: The Effect of Artificial Amalgamates on Disease Diagnosis

Descriptive Information	Amalgamate		
	Vanilla	Sparse	Dense
Mean	81.69%	74.51%	85.37%
Range	1.60%	2.17%	2.75%
Minimum Value	81.07%	73.59%	84.13%
Maximum Value	82.67%	75.66%	86.88%
Variance	2.06e(-5)	2.98e(-5)	5.73e(-5)
Standard Deviation	4.54e(-3)	5.46e(-3)	7.57e(-3)
1SD	81.66-81.69	74.50-74.52	85.36-85.38
2SD	81.68-81.69	74.49-74.52	85.35-85.39
3SD	81.68-81.70	74.49-74.53	85.35-85.39
Number	25	25	25
Results of the t-test			
Vanilla vs. Sparse $t = 359.16$ $p < 0.01$			
Vanilla vs. Dense $t = 167.25$ $p < 0.01$			
Sparse vs. Dense $t = 475.79$ $p < 0.01$			
At $df = 48$, $\alpha = 0.01$, table-$t = 2.407$ for significance			

Three t-tests calculated at a 0.01 level of significance with 48 degrees of freedom were used to compile the data collected. A null hypothesis stating the three amalgamates would have no significant difference in accuracy was formulated. A table-t value of 2.407 was used. All comparisons of vanilla vs. sparse, vanilla vs. dense, and sparse vs. dense were statistically significant because the table-t value was less than all calculated-t values. The paired calculated-t and significance values can be seen in tables 2 and 3. The data was statistically significant, with a greater than 99% confidence in the data's significance being void of chance and error. The null hypothesis was rejected in favor of the research hypothesis. Interestingly, it was found that the increased synaptic weights within the networks better compiled the images regardless of their respective acuity.

A new hybrid diagnosis algorithm was invented in this research. It used more advanced techniques to increase the accuracy. The model achieved superior classification accuracy when differentiating healthy and COVID-19 cases, as can be seen when it was compared with the amalgamates in graph 1. It was extended to other diseases. The bootstrapped mean squared error between the classes can be seen in graph 2. All five classes had a pseudo-Gaussian distribution of error. The prediction statistics of the model when assessed by a 2x2 confusion matrix can be seen in contingency tables 1-11. The model scored accuracy, sensitivity, specificity, and precision greater than 90% for Coronavirus, Tuberculosis, Carcinoma and Pneumonia. The model was then also used to differentiate the subtypes and malignancy of Carcinomas and Pneumonia infection types.

Accuracies between 96-99% were achieved for all of them. Other metrics from the confusion matrix (e.g. fall-out ratio, positive likelihood ratio, negative likelihood ratio, diagnostic odds ratio) were omitted from this paper because of the space limit. The model had very low false positive and false negative rates while delivering state-of-the-art performance. The receiver operating characteristic curve analyses were omitted from the paper due to space limitations. The model was also capable of parsing thousands of images in a timeframe of under an hour on both i3 and i7 computers without external graphics processing devices or cloud server access. The detailed analysis of the temporal parameters was omitted because of the space limit.

4 Conclusion

The purpose of this experiment was to determine the effect of different computational amalgamates on identifying airborne diseases using medical imaging. Vanilla, sparse, and dense amalgamates were trained to identify COVID-19 using CT scans and x-rays. The research hypothesis stated the dense amalgamates would be the most accurate. According to t-tests calculated at a 0.01 level with 48 degrees of freedom, the null hypothesis was rejected in favor of the research hypothesis. It was found that of the three amalgamates, the dense arrangement performed the best.

A new hybrid diagnosis model invented in this research performed the best by far. It showed superior classification capability than all three amalgamates and models proposed in other research. It identified COVID-19 at a 99.36% accuracy. The model was extended to other diseases with pathogenic effects prominent in chest x-rays. It correctly identified Coronavirus, Tuberculosis, Carcinoma, and Pneumonia from 96.93-99.36% accuracy. It was further extended

to differentiate Carcinoma (i.e. Adenocarcinoma, Squamous Cell, and Large Cell) and Pneumonia (i.e. Viral and Bacterial) subtypes. The model incorporates the dense amalgamates with more advanced artificial intelligence algorithms. It is a semi-supervised deep-learning model augmented with convolutional neural-networks isolation forests, and support vector machines, which are algorithms found in research to accelerate image classification (Albawi and Mohammed, 2017; Mensi et al, 2021; Sapthagirivasan and Anburajan, 2013). It's efficiency is attributed to the one-vs-everything design, which allows for scan customizations by splitting the initial multidimensional classifications into many binary classifications.

A possible reason for the dense amalgamate's performance is that more neurons in the network were available to compile the pixel values of an image. The increased synaptic weights were correlated to each amalgamate's performance. This logic would also explain why the sparse amalgamate delivered the worst performance. In the hybrid model built here, the convolution and pooling functions greatly reduced the amount of pixel values that were necessary to make a classification. Additionally, support vector machines have been shown to be effective when making classifications in extreme situations, and since the images were grouped in a one-vs-everything learning framework, the classification accuracy was very high.

Other researchers and engineers have used dense multilayer perceptrons to classify images in the past. Coronavirus has been identified at high accuracy in other studies as well (Rahimzadeh and Attar, 2020; Wang et al, 2020). The model developed in this research was capable of identifying four airborne diseases at state-of-the-art performance. Convolutional neural-networks were also used in these applications. However, most of these used premade engines such as GoogLeNet, ResNet-50, InceptionV3, DenseNet-201, AlexNet, etc (Krizhevsky A, 2012). These engines have higher computational cost (Xia et al, 2020). The convolutional neural-network used here was developed as a custom architecture specialized for the problem presented in the rationale. It is much lighter in comparison to these premade engines (Krizhevsky A, 2012). This means it can run heavy workloads faster without the need of a GPU or cloud server (Xia et al, 2020). In testing, it was found that thousands of images could be parsed through the model in under a minute.

For reference, this was possible on a computer without an i9 processor or GPU. Most commissioned computers in hospitals also run without GPUs. Due to this research taking a one-vs-everything adaptation, the model consists of a family of feature extractors all mapped onto support vector machines. This makes the model far more integrative than solutions proposed in other research, which mostly classified multiple diseases using one large multilayer perceptron. Electronic health record software such as Allscripts, Epic, and Cerner are commonly used by medical professionals during diagnostic procedures (Shen et al, 2019). The design of the model invented here would allow for certain extractors to be turned off during testing to better align with the differential diagnosis thinking process that many physicians use, which would be more computationally conservative than past attempts at automatic disease diagnosis algorithms (Hani et al, 2021).

Some possible sources of error in this project come from the datasets used. Despite all the scans being verified by medical professionals, there could have been errors in sorting them before their publications. In addition, the datasets were somewhat lopsided. Certain classes had many more images than others, but all classes had at least five hundred images. These flaws may have resulted in mild overfitting (Rice et al, 2020). Another error could have been in the specialized simulation used. The autoencoding networks could have been better optimized to have lower error. A generative adversarial network, which fabricates data by training a pair of multilayer perceptrons using dual-channeled backpropagation, would have been a better fit to the simulation system (Radford et al, 2016; Zhang et al, 2017).

Using machine-learning and medical imaging, the hybrid model fabricated here delivered state-of-the-art performance compared to past research. This approach is more conservative than other methods. Because of this, it is more suited for underdeveloped or remote regions due to it not needing a GPU or cloud server to parse hundreds of scans at once. Unlike other biomarkers, the model can operate without the presence of doctors or researchers to analyze the results, but the spatiotemporal parameters can be refined to work with real-time scans (Arbabshirani et al, 2018). In the modern era, medical professionals use software, and integrating models such as the one developed here into the aforementioned software could significantly boost diagnostic procedures. The model can also identify four different diseases and five subtypes opposed to only one. In addition, the testing done through the specialized simulation was more advanced than regular cross-validation testing because it utilized a novel unsupervised image generation system and a 2x2 confusion matrix. This challenged the model further to predict more randomized cases.

In the future, different applications of graph theory could be explored to better the performance of the hybrid model. Gated recovery units and long-short term memory algorithms are variants of recurrent neural-networks that are often used to track time series data (Horvath et al, 2018; Hochreiter and Schmidhuber, 1997). These could possibly be used in conjunction with the model to track disease progression. Another application could be extending the model to identify other diseases in different anatomical structures. Examples would be training the model to identify Alzheimer's in the brain or Osteoporosis in the vertebral column (Lee et al, 2018; Sapthagirivasan and Anburajan, 2013).

5 Citations

[1] Albawi S. and Mohammed T. (2017, August 21st). Understanding of a Convolutional Neural Network. International Conference on Engineering and Technology (ICET). Retrieved on June 9th 2021 from doi: 10.1109/ICEngTechnol.2017.8308186

[2] Arbabshirani M, et al (2018). Advanced machine learning in action: identification of intracranial hemorrhage on computed tomography scans of the head with clinical workflow integration. NPJ Digital Medicine, 1. Retrieved on August 15th 2021 from doi: 10.1038/s41746-017-0015-z

[3] Baker B, et al. (2017, March 22nd). Designing Neural Network Architectures using Reinforcement Learning. arXiv of Cornell University. Retrieved on June 9th 2021 from URL: https://arxiv.org/abs/1611.02167

[4] Hani C, et al. (2020). COVID-19 pneumonia: A review of typical CT findings and differential diagnosis. Diagnostic and Interventional Imaging, 101, 263-268. Retrieved on August 15th 2021 from doi: 10.1016/j.diii.2020.03.014

[5] He F, et al. (2020, March 2nd). Coronavirus disease 2019: What we know? Wiley Journal of Medical Virology. Retrieved on August 13th 2021 from doi: 10.1002/jmv.25766

[6] Hochreiter S. and Schmidhuber J. (1997, November 15th). Long Short-Term Memory. Neural Computation, 9, 1735-1780. Retrieved on August 13th 2021 from doi: 10.1162/neco.1997.9.8.1735

[7] Horvath A, et al. (2018). Spinal Cord Gray Matter-White Matter Segmentation on Magnetic Resonance AMIRA Images with MD-GRU. arXiv of Cornell University. Retrieved on August 15th 2021 from doi: 10.1007/978-3-030-13736-6_1

[8] Krizhevsky A, et al. (2012). ImageNet classification with deep convolutional neural networks. Communications of the ACM, 60, 84 - 90. Retrieved on August 15th 2021 from doi: 10.1145/3065386

[9] Mensi A, et al. (2021). Proximity Isolation Forests. 2020 25th International Conference on Pattern Recognition (ICPR), 8021-8028. Retrieved on August 15h 2021 from doi: 10.1109/ICPR48806.2021.9412322

[10] Lee J, et al. (2018, July 13th). Osteoporosis detection in panoramic radiographs using a deep convolutional neural network-based computer-assisted diagnosis system: a preliminary study. Dento maxillo facial radiology, 20170344. Retrieved on August 15th 2021 from doi: 10.1259/dmfr.20170344

[11] Liu Q, et al. (2020, October 21st). A Two-Dimensional Sparse Matrix Profile DenseNet for COVID-19 Diagnosis Using Chest CT Images. IEEEAcess. Retrieved on June 9th 2021 from URL: https://ieeexplore.ieee.org/stamp/stamp.jsp?arnumber=9268138

[12] Liu Y, et al. (2017). A method for multi-class sentiment classification based on an improved one-vs-one (OVO) strategy and the support vector machine (SVM) algorithm. Information Sciences, 394, 38-52. Retrieved on August 13th 2021 from doi: 10.1016/j.ins.2017.02.016

[13] Radford A, et al. (2016). Unsupervised Representation Learning with Deep Convolutional Generative Adversarial Networks. arXiv of Cornell University. Retrieved on August 15th 2021 from URL: https://arxiv.org/pdf/1511.06434.pdf

[14] Rahimzadeh M. and Attar A. (2020, May 21st). A modified deep convolutional neural network for detecting COVID-19 and pneumonia from chest X-ray images based on the concatenation of Xception and ResNet50V2. Informatics in Medicine Unlocked, 19, 360-369. Retrieved on August 13th 2021 from doi: 10.1016/j.imu.2020.100360

[15] Rice L, et al. (2020). Overfitting in adversarially robust deep learning. ICML. Retrieved on August 15th 2021 from URL: https://arxiv.org/pdf/2002.11569.pdf

[16] Sapthagirivasan V. and Anburajan M. (2013). Diagnosis of osteoporosis by extraction of trabecular features from hip radiographs using support vector machine: An investigation panorama with DXA. Computers in biology and medicine, 43(11). Retrieved on August 13th 2021 from doi: 10.1016/j.compbiomed.2013.09.002

[17] Simoneuax R. and Shafer S. (2020). Current State of COVID Testing. In the Know, 84, 8-9. Retrieved on August 13th 2021 from doi: 10.1097/01.asm.0000716944.70366.26

[18] Shen Z, et al. (2019). A systematic review on open source clinical software on GitHub for improving software reuse in smart healthcare. Applied Sciences, 9, 150. Retrieved on August 15th 2021 from doi: 10.3390/APP9010150

[19] Wang L, et al. (2020, Nov 11th). COVID-Net: a tailored deep convolutional neural network design for detection of COVID-19 cases from chest X-ray images. Scientific Reports, 10(1). Retrieved on August 13th 2021 from doi: 10.1038/s41598-020-76550-z

[20] Xia Q, et al. (2020). Roadmap on emerging hardware and technology for machine learning. Nanotechnology. Nanotechnology, 32. Retrieved on August 15th 2021 from doi: 10.1088/1361-6528/aba70f

[21] Xu J, et al. (2019, July 11th). Three-way confusion matrix for classification: A measure driven view. Information Science, 507, 772-794. Retrieved on August 13th 2021 from doi: 10.1016/J.INS.2019.06.064

[22] Xu W, et al. (2019). Adversarially Approximated Autoencoder for Image Generation and Manipulation. IEEE Transactions on Multimedia, 21, 2387-2396. Retrieved on August 15th 2021 from doi: 10.1109/TMM.2019.2898777

[23] Zhang H, et al. (2017). StackGAN: Text to Photo-Realistic Image Synthesis with Stacked Generative Adversarial Networks. 2017 IEEE International Conference on Computer Vision (ICCV), 5908-5916. Retrieved on August 15th 2021 from doi: 10.1109/ICCV.2017.629

[24] Zhang J, et al. (2017, January 4th). Diagnostic Method of Diabetes Based on Support Vector Machine and Tongue Images. BioMed Research International. Retrieved on August 13th 2021 from doi: 10.1155/2017/7961494

6 Appendix

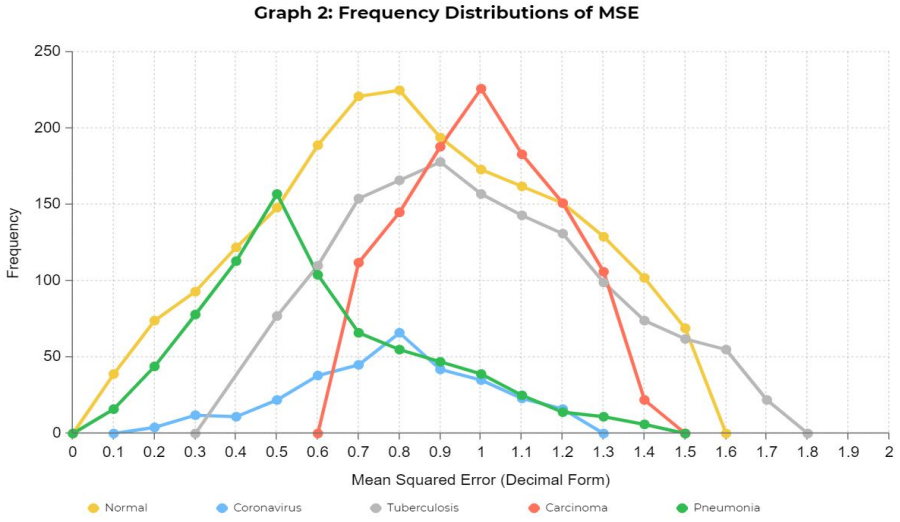

Table 2: Paired T-Tests at 0.01 Value and 48 Degrees of Freedom

	Vanilla (Control)	Sparse	Dense
Vanilla (Control)	N/A	-359.16	-167.25
Sparse	359.16	N/A	-475.79
Dense	167.25	475.79	N/A

Table 3: Paired Significances at 0.01 Value and 48 Degrees of Freedom

	Vanilla (Control)	Sparse	Dense
Vanilla (Control)	N/A	$p < 0.01$	$p < 0.01$
Sparse	$p < 0.01$	N/A	$p < 0.01$
Dense	$p < 0.01$	$p < 0.01$	N/A

Contingency Table 1: Predictions of Coronavirus

Prediction	Count
True Positives	539
True Negatives	5074
False Positives	36
False Negative	0

99.36% accuracy, 99.29% specificity, 100.00% sensitivity, 93.74% precision

Contingency Table 2: Predictions of Tuberculosis

Prediction	Count
True Positives	3347
True Negatives	4763
False Positives	149
False Negative	114

96.93% accuracy, 97.09% specificity, 96.71% sensitivity, 95.74% precision

Contingency Table 3: Predictions of Carcinoma

Prediction	Count
True Positives	861
True Negatives	403
False Positives	13
False Negative	0

98.81% accuracy, 96.86% specificity, 100.00% sensitivity, 98.13% precision

Contingency Table 4: Predictions of Pneumonia

Prediction	Count
True Positives	4214
True Negatives	5006
False Positives	67
False Negative	59

98.65% accuracy, 98.68% specificity, 98.62% sensitivity, 98.43% precision

Contingency Table 5: Predictions of Adenocarcinoma

Prediction	Count
True Positives	118
True Negatives	405
False Positives	2
False Negative	11

97.57% accuracy, 99.51% specificity, 91.47% sensitivity, 98.33% precision

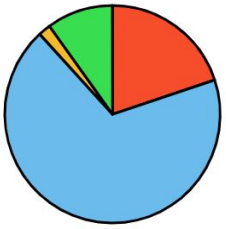

Contingency Table 6: Predictions of Squamous Cell Carcinoma

Prediction	Count
True Positives	102
True Negatives	411
False Positives	3
False Negative	4

98.65% accuracy, 99.28% specificity, 96.23% sensitivity, 97.14% precision

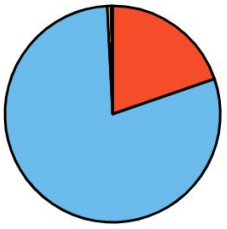

Contingency Table 7: Predictions of Malignant Carcinoma

Prediction	Count
True Positives	551
True Negatives	402
False Positives	21
False Negative	14

96.46% accuracy, 95.04% specificity, 97.52% sensitivity, 96.33% precision

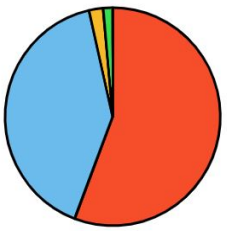

Contingency Table 8: Predictions of Bengin Carcinoma

Prediction	Count
True Positives	120
True Negatives	396
False Positives	20
False Negative	0

96.27% accuracy, 95.19% specificity, 100.00% sensitivity, 85.71% precision

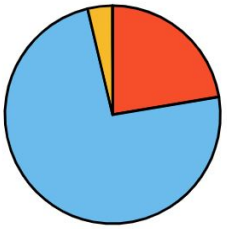

Contingency Table 9: Predictions of Large Cell Carcinoma

Prediction	Count
True Positives	69
True Negatives	406
False Positives	3
False Negative	10

97.34% accuracy, 99.27% specificity, 87.34% sensitivity, 97.34% precision

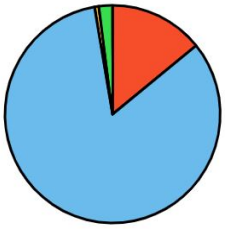

Contingency Table 10: Predictions of Viral Pneumonia

Prediction	Count
True Positives	1340
True Negatives	4944
False Positives	129
False Negative	2

97.96% accuracy, 97.46% specificity, 99.85% sensitivity, 91.22% precision

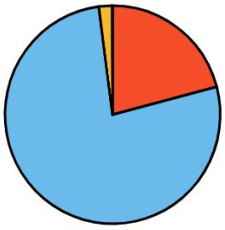

Contingency Table 11: Predictions of Bacterial Pneumonia

Prediction	Count
True Positives	4271
True Negatives	4768
False Positives	305
False Negative	2

96.72% accuracy, 93.99% specificity, 99.95% sensitivity, 93.33% precision